A fast integral sliding mode controller with an extended state observer for position control of permanent magnet synchronous motor servo systems

Jun-feng JIANG[1,2], Xiao-jun ZHOU[†‡1,2], Wei ZHAO[3], Wei LI[3], Wen-dong ZHANG[4]

¹State Key Laboratory of Fluid Power and Mechatronic Systems, Zhejiang University, Hangzhou 310027, China
²Zhejiang Province Key Laboratory of Advanced Manufacturing Technology, Zhejiang University, Hangzhou 310027, China
³Northwest Institute of Mechanical and Electrical Engineering, Xianyang 712099, China
⁴Beijing Linkstech Technology Co., Ltd, Beijing 102200, China
†E-mail: cmeesky@163.com

Abstract: Permanent magnet synchronous motor (PMSM) has been widely used in position control applications. Its performance is not satisfactory due to internal uncertainties and external load disturbances. To enhance the control performance of PMSM systems, a new method that has fast response and good robustness is proposed in this study. First, a modified integral terminal sliding mode controller is developed, which has a fast-sliding surface and a continuous reaching law. Then, an extended state observer is applied to measure the internal and external disturbances. Therefore, the disturbances can be compensated for in a feedforward manner. Compared with other sliding mode methods, the proposed method has faster response and better robustness against system disturbances. In addition, the position tracking error can converge to zero in a finite time. Simulation and experimental results reveal that the proposed control method has fast response and good robustness, and enables high-precision control.

Key words: Permanent magnet synchronous motor (PMSM); Sliding mode controller; Extended state observer; Robust control; Motion control

1 Introduction

Permanent magnet synchronous motor (PMSM) is important in high-performance servo applications (e.g., machine tools, aviation, and robots). It has advantages such as high power density, compactness, and low inertia (Zeng et al., 2002; Chen et al., 2015). Proportional-integral (PI) controller has been extensively used because of its easy implementation (Wang M et al., 2018). However, achieving satisfactory control performance of the PMSM system is unreal-

istic when a PI controller is used (Wai, 2001; Yang JQ et al., 2017), because the PMSM system is nonlinear. In addition, it is affected by external load disturbances and internal parameter variations in practical applications (Yu et al., 2005; Li et al., 2015).

To enhance the performance of PMSM servo systems, several nonlinear control methods have been proposed, such as fuzzy logic control (Chaoui and Sicard, 2012), neural network control (El-Sousy, 2010), and predictive control (Zhi et al., 2010). El-Sousy (2010, 2013) proposed an intelligent neural network control method to deal with the unmodeled parts of the PMSM model. Barkat et al. (2011) developed an adaptive fuzzy controller to eliminate the interconnection effects of the PMSM. Nguyen and Jung (2018) developed model predictive control

---

ORCID: Jun-feng JIANG, https://orcid.org/0000-0001-5201-8753; Xiao-jun ZHOU, https://orcid.org/0000-0003-2565-1398

(MPC) to guarantee the stability and robustness of surface-mounted PMSM drives. In addition, it has been verified that the MPC method has high-speed tracking capacity and low switching frequency. The above methods have improved the control performance of PMSM systems from different perspectives. However, note that the design complexity and computational burden of these methods are increased (Nguyen et al., 2018). Moreover, it is difficult to adapt these designs to position control of PMSM systems.

Sliding mode control (SMC) has been widely used because of its fast response and good robustness against uncertainties (Zhang, 2016). In general, the following three steps must be considered to design an SMC system, i.e., choosing a sliding mode surface, designing a reaching law, and determining a control law. Conventional SMC usually has a linear sliding surface (SS). Consequently, it can guarantee only asymptotic stability; i.e., the response error cannot converge to zero in a finite time. Terminal sliding mode (TSM) control possessing a nonlinear SS was introduced by Man et al. (1994). Unlike conventional SMC, the TSM method can guarantee a finite-time convergence. However, the control input of TSM is singular in some cases. To solve this problem, a non-singular TSM (NTSM) was proposed by Feng Y et al. (2002). However, the reaching law of NTSM is discontinuous, and therefore the chattering phenomenon is inevitable. The boundary layer method was adopted to reduce the chattering level, but it can lead to asymptotic stability. Yu et al. (2005) developed a continuous NTSM (CNTSM) by replacing the discontinuous reaching law of NTSM with a continuous one (Al-Ghanimi et al., 2017). As a result, the chattering and singularity problems, which are the two main problems of the TSM control scheme (Feng Y et al., 2014), are solved to some extent.

However, there are still two main issues relevant to the use of the CNTSM method:

1. The nonlinear SS has much slower convergence speed compared with a linear one. This phenomenon occurs especially when the system state is far away from the equilibrium.

2. Prior knowledge of the boundary of the lumped disturbance is required to obtain enough robustness. However, this is impossible in real applications, so the robustness is not satisfactory and steady-state fluctuation is inevitable (Yang J et al., 2013).

To enhance the system performance in the presence of disturbances, an extended state observer (ESO) has been developed (Han, 2009). It has been successfully applied in motion control of PMSM (Feng G et al., 2004; Su YX et al., 2005; Bobtsov et al., 2017), robotic systems (Su JB et al., 2004), and machining processes (Wu et al., 2007). It concerns the lumped disturbance as a new system state and can estimate both disturbance and states (Saadaoui et al., 2017). Therefore, feedforward compensation can be introduced into the controller design. Jiang and Zhou (2019) proposed a robust and fast TSM (RFTSM) control method by combining fast TSM control with the ESO method. Simulation results showed that the RFTSM method has fast response and good robustness, and enables high-precision control in position tracking control of PMSM drives. However, experimental verifications are absent and positioning performance of PMSM drives is not verified. In addition, the singularity problem is not avoided in the RFTSM design.

In this study, a fast, continuous, integral sliding mode (FCISM) controller is proposed for PMSM systems. Combining FCISM control with the ESO, we propose a composite robust FCISM (RFCISM) method. The proposed RFCISM method retains the advantages of RFTSM, such as finite-time stability and disturbance rejection capability. In addition, it can start on the SS, so the reaching phase is eliminated and fast response can be guaranteed. In addition, RFCISM solves the singularity problem in RFCISM control effectively. Simulation and experimental results are provided to validate the effectiveness of the proposed method.

2 Controller design

A second-order nonlinear dynamic system with external disturbances can be expressed as

$$\begin{cases} \dot{x}_1 = x_2, \\ \dot{x}_2 = g(\boldsymbol{x})u + f(\boldsymbol{x}) + d, \end{cases} \quad (1)$$

where $\boldsymbol{x}=[x_1, x_2]^{\mathrm{T}}$ is the system state vector, $g(\boldsymbol{x})$ and $f(\boldsymbol{x})$ the nonlinear functions of $\boldsymbol{x}$, d the lumped disturbance consisting of internal uncertainties and external load disturbances, and u the control input signal.

Let x_{ref} be the position reference and define the tracking error as $e=x_1-x_{\mathrm{ref}}$. The control purpose is to obtain a control input u such that the system position output x_1 tracks the position reference fast and precisely.

2.1 FCISM controller design

SS of NTSM introduced in Feng Y et al. (2002) can be described as

$$s = e + \beta \dot{e}^{m/n} = 0, \qquad (2)$$

where $0<\beta<1$ is a design constant and m and n are positive odd integers satisfying $n<m<2n$. Then, the control input u does not have terms with negative fractional powers, which may lead to singularity. However, the reaching law of NTSM has a switching term expressed as follows:

$$\dot{s} = -\eta \operatorname{sgn}(s), \qquad (3)$$

where $\eta>0$ is a constant to be designed and $\operatorname{sgn}(\cdot)$ the sign function. It is evident that this type of reaching law will lead to a chattering control input. To alleviate the chattering phenomenon, the boundary layer approach (Baik et al., 2000) is incorporated into NTSM. However, choosing the width of the boundary layer is not easy, and the performance of disturbance rejection is sacrificed (Wang HM et al., 2017).

Retaining the non-singular and finite-time SS, CNTSM control is proposed by replacing the discontinuous reaching law with a continuous one, expressed as follows:

$$\dot{s} = -k_1 s - k_2 \mid s \mid^{q_0/p_0} \operatorname{sgn}(s), \qquad (4)$$

where k_1 and k_2 are positive design constants and p_0 and q_0 are positive odd integers satisfying $p_0>q_0$. As a result, the derived control input contains no negative fractional power, and therefore it is non-singular. Moreover, it is continuous, so the chattering phenomenon is eliminated. Therefore, according to Eq. (2), we have

$$\dot{e} = -e^{n/m} / \beta^{n/m}. \qquad (5)$$

It is obvious that the absolute value of $\dot{e}$ is much

smaller than $\dot{e} = -e^{m/n} / \beta^{m/n}$ when e is far away from zero. In other words, the convergence speed of a nonlinear SS is slower than that of a linear one. Note that this result completely reverses when e is close to zero.

A fast integral SS is designed as follows:

$$s = \dot{e} + \beta_1 e^{\gamma_1} + \alpha_{\mathrm{I}} \int_0^t e^{\gamma_2}(\tau)\mathrm{d}\tau, \qquad (6)$$

where β_{I}, α_{I}, γ_1, and γ_2 are positive parameters with $\gamma_1>1$. To obtain a high convergence speed, γ_2 is defined as

$$\gamma_2 = \begin{cases} m_{\mathrm{I}}/n_{\mathrm{I}}, & \mid e \mid \geq \delta, \\ n_{\mathrm{I}}/m_{\mathrm{I}}, & \mid e \mid < \delta, \end{cases} \qquad (7)$$

where m_{I} and n_{I} are positive odd integers with $m_{\mathrm{I}}>n_{\mathrm{I}}$ and δ is the switching value. Combining the SS in Eq. (6) and the reaching law in Eq. (4), a novel FCISM method for system (1) is obtained as follows:

$$u_0 = -g^{-1}(\boldsymbol{x})\Big[f(\boldsymbol{x}) + \beta_{\mathrm{I}}\gamma_1 e^{\gamma_1-1}\dot{e} + \alpha_{\mathrm{I}}e^{\gamma_2} \\ -\ddot{x}_{\mathrm{ref}} + k_{1\mathrm{I}}s + k_{2\mathrm{I}} \mid s \mid^{q_{0\mathrm{I}}/p_{0\mathrm{I}}} \operatorname{sgn}(s)\Big], \qquad (8)$$

where $k_{1\mathrm{I}}$, $k_{2\mathrm{I}}$, $q_{0\mathrm{I}}$, and $p_{0\mathrm{I}}$ are parameters of the reaching law of the FCISM controller with $p_{0\mathrm{I}}>q_{0\mathrm{I}}$. $q_{0\mathrm{I}}$ is modified as follows for finite-time stabilization:

$$\begin{cases} q_{0\mathrm{I}} > 0, & \mid s \mid \geq 1, \\ q_{0\mathrm{I}} = 0, & \mid s \mid < 1. \end{cases} \qquad (9)$$

Remark 1 SS of the conventional integral terminal sliding mode (ITSM) controller in Chiu (2012) can be expressed as

$$s_{\mathrm{c}} = \dot{e} + \beta_{\mathrm{c}}e + \alpha_{\mathrm{c}} \int_0^t e^{n_{\mathrm{c}}/m_{\mathrm{c}}}(\tau)\mathrm{d}\tau, \qquad (10)$$

where β_{c} and α_{c} are positive parameters and n_{c} and m_{c} are positive odd integers. When $s_{\mathrm{c}}=s=0$ and e is far away from zero, Eq. (11) can be derived from Eq. (6):

$$\dot{e} = -\beta_{\mathrm{I}}e^{\gamma_1} - \alpha_{\mathrm{I}} \int_0^t e^{m_{\mathrm{I}}/n_{\mathrm{I}}}(\tau)\mathrm{d}\tau, \qquad (11)$$

and Eq. (12) can be derived from Eq. (10):

$$\dot{e} = -\beta_{\mathrm{c}}e - \alpha_{\mathrm{c}}\int_0^t e^{n_{\mathrm{c}}/m_{\mathrm{c}}}(\tau)\mathrm{d}\tau. \tag{12}$$

Assume $\beta_{\mathrm{I}}=\beta_{\mathrm{c}}$ and $\alpha_{\mathrm{I}}=\alpha_{\mathrm{c}}$. We can see that the absolute value of $\dot{e}$ in Eq. (12) is smaller than that in Eq. (11) when e is far away from zero. In other words, the convergence speed of the conventional method is slower than that of the proposed method when e is far away from zero. This can also be validated by the simulations and experiments in this study.

Remark 2 Non-singularity and fast response are two main advantages of the ITSM controller. We can enable the system states to start on $s=0$ by adjusting the initial value of $\int_0^t e^{\gamma_2}(\tau)\mathrm{d}\tau$. Therefore, the reaching phase can be eliminated and fast response can be obtained. In addition, we can see from Eq. (8) that there is no negative fractional power in the control law. In other words, the proposed control scheme is non-singular.

2.2 RFCISM controller design

To improve the disturbance rejection property of this system, an ESO is incorporated to estimate the lumped disturbance. The estimated disturbance acts as a feedforward compensation term.

According to Miklosovic and Gao (2004), a second-order linear ESO for system (1) can be designed as

$$\begin{cases} \dot{\hat{x}}_2 = \hat{d} - 2p(\hat{x}_2 - x_2) + g(x)u, \\ \dot{\hat{d}} = -p^2(\hat{x}_2 - x_2), \end{cases} \tag{13}$$

where $\hat{x}_2$ and $\hat{d}$ are the estimates of x_2 and d, respectively, and $-p$ is the desired pole of the ESO with $-p<0$. The estimated disturbance $\hat{d}$ will converge to the real lumped disturbance d asymptotically. The estimation error is defined as

$$\tilde{d} = \hat{d} - d. \tag{14}$$

Note that $\hat{d}$ usually contains some bounded noise in real applications, and thus the estimation error is bounded by a constant as follows:

$$\left|\tilde{d}\right| < \varepsilon, \tag{15}$$

where ε is a positive value.

Combining FCISM and ESO, the RFCISM method is developed as follows:

$$u = u_0 - g^{-1}(x)\hat{d}. \tag{16}$$

Compared with control law (8), control law (16) has a disturbance compensation term. Therefore, it has a better disturbance rejection property and a smaller steady-state fluctuation.

Theorem For system (1), if the control input u is designed according to Eq. (16) and the gain satisfies $k_{2\mathrm{I}}{\geq}\varepsilon$, the tracking error e and its first-order derivative $\dot{e}$ will converge to zero in a finite time.

Proof Choosing a Lyapunov function as

$$V = \frac{1}{2}s^2, \tag{17}$$

the derivative of the Lyapunov function is

$$\begin{aligned} \dot{V} &= s\dot{s} = s\left(\ddot{e} + \beta_{\mathrm{I}}\gamma_1 e^{\gamma_1-1}\dot{e} + \alpha_{\mathrm{I}}e^{\gamma_2}\right) \\ &= s\left[g(x)u + f(x) + d - \ddot{x}_{\mathrm{ref}} + \beta_{\mathrm{I}}\gamma_1 e^{\gamma_1-1}\dot{e} + \alpha_{\mathrm{I}}e^{\gamma_2}\right]. \end{aligned} \tag{18}$$

Substituting Eq. (16) into Eq. (18) yields

$$\begin{aligned} \dot{V} &= s\Big\{g(x)\Big[-g^{-1}(x)\Big(f(x) + \beta_{\mathrm{I}}\gamma_1 e^{\gamma_1-1}\dot{e} + \alpha_{\mathrm{I}}e^{\gamma_2} \\ &\quad -\ddot{x}_{\mathrm{ref}} + k_{1\mathrm{I}}s + k_{2\mathrm{I}}\mid s\mid^{q_{0\mathrm{I}}/p_{0\mathrm{I}}}\mathrm{sgn}(s) + \hat{d}\Big)\Big] \\ &\quad + f(x) + d - \ddot{x}_{\mathrm{ref}} + \beta_{\mathrm{I}}\gamma_1 e^{\gamma_1-1}\dot{e} + \alpha_{\mathrm{I}}e^{\gamma_2}\Big\} \\ &= s\Big(-k_{1\mathrm{I}}s - k_{2\mathrm{I}}\mid s\mid^{q_{0\mathrm{I}}/p_{0\mathrm{I}}}\mathrm{sgn}(s) - \tilde{d}\Big). \end{aligned} \tag{19}$$

If $|s|{\geq}1$, Eq. (19) can be rewritten as

$$\begin{aligned} \dot{V} &= -k_{1\mathrm{I}}s^2 - k_{2\mathrm{I}}\mid s\mid^{q_{0\mathrm{I}}/p_{0\mathrm{I}}}s\,\mathrm{sgn}(s) - s\tilde{d} \\ &= -k_{1\mathrm{I}}s^2 - k_{2\mathrm{I}}\mid s\mid^{q_{0\mathrm{I}}/p_{0\mathrm{I}}}\mid s\mid -s\tilde{d} \\ &\leq -k_{1\mathrm{I}}s^2 - k_{2\mathrm{I}}\mid s\mid^{q_{0\mathrm{I}}/p_{0\mathrm{I}}+1} + \mid s\mid\left|\tilde{d}\right| \\ &= -k_{1\mathrm{I}}s^2 - \left(k_{2\mathrm{I}}\mid s\mid^{q_{0\mathrm{I}}/p_{0\mathrm{I}}} - \left|\tilde{d}\right|\right)\mid s\mid \\ &\leq -k_{1\mathrm{I}}s^2 - (k_{2\mathrm{I}} - \varepsilon)\mid s\mid\leq 0. \end{aligned} \tag{20}$$

If $|s|<1$, Eq. (19) can be rewritten as

$$\begin{aligned} \dot{V} &= -k_{1\mathrm{I}}s^2 - k_{2\mathrm{I}}\mid s\mid^{q_{0\mathrm{I}}/p_{0\mathrm{I}}}s\,\mathrm{sgn}(s) - s\tilde{d} \\ &= -k_{1\mathrm{I}}s^2 - k_{2\mathrm{I}}\mid s\mid -s\tilde{d} \\ &\leq -k_{1\mathrm{I}}s^2 - k_{2\mathrm{I}}\mid s\mid + \mid s\mid\left|\tilde{d}\right| \\ &= -k_{1\mathrm{I}}s^2 - \left(k_{2\mathrm{I}} - \left|\tilde{d}\right|\right)\mid s\mid\leq 0. \end{aligned} \tag{21}$$

Therefore, the condition for Lyapunov stability is satisfied. This completes the proof.

3 Application in permanent magnet synchronous motor servo systems

Taking the rotor coordinates d-q as the reference coordinates, the mathematical model of a surface-mounted PMSM can be expressed as follows (Li and Liu, 2009):

$$\begin{cases} u_d = L_s \dot{i}_d - \omega_r L_s i_q + R_s i_d, \\ u_q = L_s \dot{i}_q + \omega_r L_s i_d + R_s i_q + \psi_r \omega_r, \\ T_e = K_t i_q, \\ \dfrac{J}{n_p} \dot{\omega}_r = T_e - \dfrac{B}{n_p} \omega_r - T_L, \end{cases} \quad (22)$$

where u_d and u_q are the axis stator voltages, i_d and i_q the axis stator currents, L_s the stator inductance, R_s the stator resistance, ψ_r the normal value of flux linkage of rotors, ω_r the electrical angular velocity of rotors, T_e the electrical magnetic torque, n_p the number of pole pairs, K_t the torque constant, J the system moment of inertia, B the viscous friction coefficient, and T_L the load torque.

The conventional vector control for PMSM includes a position loop, a speed loop, and two current loops. In this study, the position loop and speed loop are unified (called the position-speed loop). The diagram of the proposed RFCISM for PMSM is shown in Fig. 1. Usually, to attenuate the couplings between speed and current, the d-axis reference current i_d^* is set to 0. So, taking the angular position and velocity as the system state variables, the state-space model can be expressed as

$$\begin{cases} \dot{\theta}_r = \omega_r, \\ \dot{\omega}_r = \dfrac{n_p K_t}{J} i_q - \dfrac{B}{J} \omega_r - \dfrac{n_p}{J} T_L, \end{cases} \quad (23)$$

where θ_r and ω_r represent the electrical angular position and velocity of rotors, respectively. Adopting the control input i_q^*, the motor state-space model can be rewritten as

$$\begin{cases} \dot{\theta}_r = \omega_r, \\ \dot{\omega}_r = a i_q^* + b \omega_r + d, \end{cases} \quad (24)$$

which is similar to system (1) in form, where $a = n_p K_t / J$, $b = -B/J$, and $d = -\dfrac{n_p K_t}{J} (i_q^* - i_q) - \dfrac{n_p}{J} T_L$.

For comparison, the CNTSM controller is employed for PMSM systems, and its control law can be described as

$$i_q^* = -a^{-1} \left(b\omega_r + k_1 s + k_2 s^{q_0/p_0} - \ddot{\theta}_{\text{ref}} + \beta^{-1} \frac{n}{m} \dot{e}^{2-m/n} \right), \quad (25)$$

where θ_{ref} is the position reference, $e = \theta_r - \theta_{\text{ref}}$, $\dot{e} = \omega_r - \dot{\theta}_{\text{ref}}$, and s is designed according to Eq. (2).

According to Eq. (8), the FCISM control law for PMSM can be expressed as
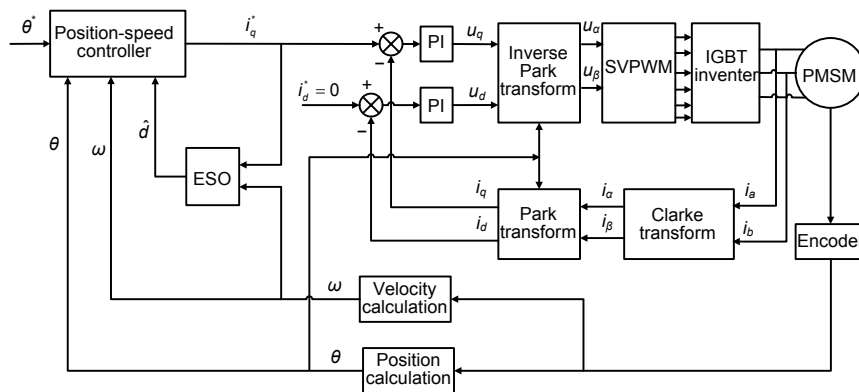

Fig. 1 Diagram of the proposed robust, fast, continuous, integral sliding mode (RFCISM) for permanent magnet synchronous motor (PMSM)
SVPWM: space vector pulse width modulation; IGBT: insulated gate bipolar transistor; ESO: extended state observer

$$i_q^* = -a^{-1} \Big[b\omega_r + \beta_1 \gamma_1 e^{\gamma_1 - 1} \dot{e} + \alpha_1 e^{\gamma_2}$$
$$-\ddot{\theta}_{ref} + k_{1I} s + k_{2I} \mid s \mid^{q_{01}/p_{01}} \mathrm{sgn}(s) \Big], \tag{26}$$

where s is designed according to Eq. (6). According to Eq. (16), the RFCISM control law can be expressed as

$$i_q^* = -a^{-1} \Big[b\omega_r + \beta_1 \gamma_1 e^{\gamma_1 - 1} \dot{e} + \alpha_1 e^{\gamma_2} - \ddot{\theta}_{ref}$$
$$+ k_{1I} s + k_{2I} \mid s \mid^{q_{01}/p_{01}} \mathrm{sgn}(s) + \hat{d} \Big]. \tag{27}$$

4 Results and discussion

To verify the performance of the proposed method, simulations and experiments are carried out in MATLAB/Simulink and a digital signal processing (DSP) based test environment, respectively. For comparison, three methods, i.e., CNTSM, FCISM, and RFCISM, are applied to the PMSM position control system. Saturation limits of the control input i_q^* are ±30 A. Note that every control algorithm obtains relatively good performance by adjusting its parameters. Parameters of the PMSM system are shown in Table 1.

Table 1 Parameters of the PMSM system

Parameter	Value
Rated power (Kw)	1.5
Rated torque (N·m)	14.32
Rated speed (rad/s)	1000
Stator resistance (Ω)	1.79
Number of pole pairs	4
Torque constant (N·m/A)	2.45
System inertia (kg·m^2)	1.792×10^{-3}
Viscous coefficient (N·m·s/rad)	9.403×10^{-5}
Stator inductance (H)	6.68×10^{-3}
Flux linkage (Wb)	0.4083

4.1 Simulation results

The PMSM tracking system under the afore-mentioned three control schemes is simulated by MATLAB/Simulink R2017a. Position reference is $\theta_{ref} = 30\cos[\pi/(2t)]°$, which can lead to a relatively good performance of the CNTSM controller. To demonstrate the disturbance rejection ability of the proposed method, external load torque $T_L = 30$ N·m is added at $t = 2$ s and removed at $t = 3$ s. PI parameters of the two current loops are the same, i.e., the proportional gain $K_p = 150$ and integral gain $K_i = 750$.

Parameters of CNTSM are selected as follows: $k_1 = k_2 = 200$, $q_0 = 1$, $p_0 = 5$, $m = 9$, $n = 5$, and $\beta = 1/500$. Simulation results of CNTSM are shown in Fig. 2. We can see that the tracking error converges to zero in a finite time and that there is no singularity in the control input i_q^*. However, the convergence speed is slow. In addition, there are obvious fluctuations in Fig. 2a when the external disturbance is added or removed.
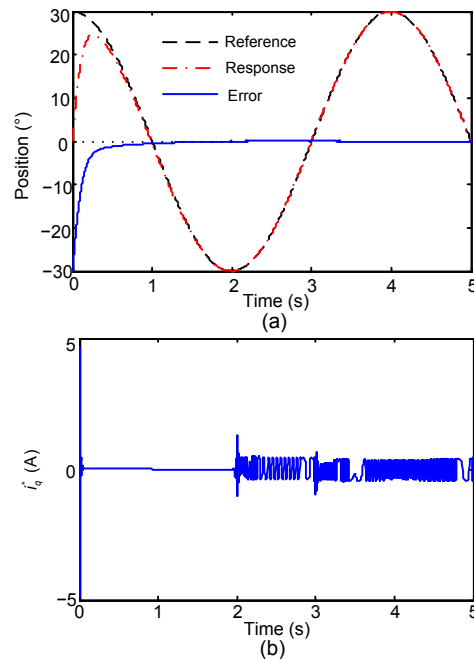
Fig. 2 Tracking performances of CNTSM in simulation: (a) position response; (b) control input i_q^*

Parameters of FCISM in the linear phase are set as follows: $\beta_I = 1/18$, $\alpha_I = 50$, $\gamma_I = 1.7$, $k_{1I} = k_{2I} = 300$, $n_I = 1$, $m_I = 5$, $q_{0I} = 1$, $p_{0I} = 5$, and $\delta = 0.03$. Simulation results of FCISM are shown in Fig. 3. It is obvious that the convergence time of FCISM is much shorter than that of CNTSM. However, the fluctuations of the tracking error still exist due to external disturbances. Moreover, we can see from Fig. 3b that the control input i_q^* does not suppress the disturbance effectively.

For RFCISM, the pole of ESO is $-p = -50\,000$ and other parameters are the same as those of FCISM. Simulation results of RFCISM are shown in Fig. 4. We can see that fast response and high-precision control are achieved. Additionally, the disturbance effect is eliminated effectively. We can see from

Fig. 5 that the ESO can estimate the disturbance accurately. Hence, the absolute value of the control input can increase remarkably to depress the
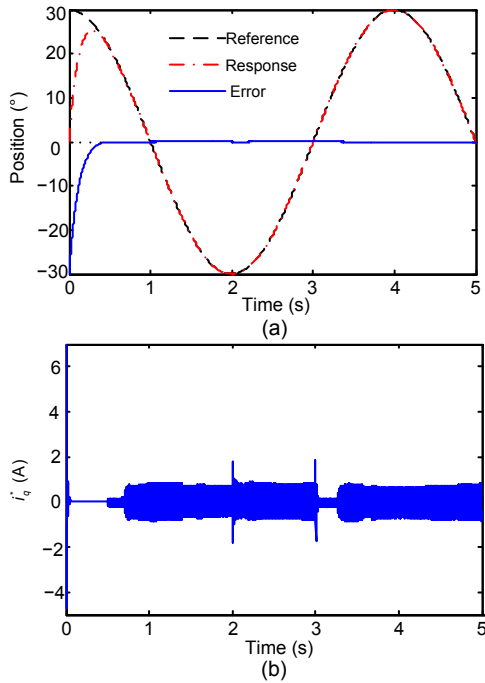

Fig. 3 Tracking performances of FCISM in simulation: (a) position response; (b) control input i_q^*
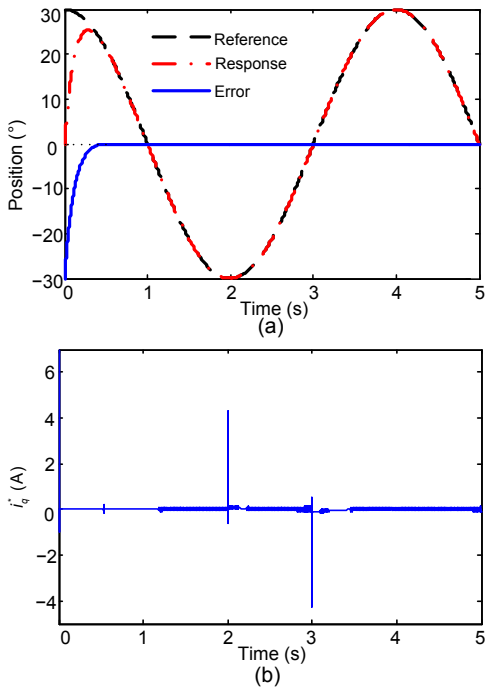

Fig. 4 Tracking performances of RFCISM in simulation: (a) position response; (b) control input i_q^*

disturbances. Fig. 6 shows the position response under RFCISM with perturbation in the system inertia. $J_0=1.792\times10^{-3}$ kg·m^2 is the initial value of the system inertia. It can be seen that the transient response remains fast and accurate, regardless of the internal parameter variations. In addition, the tracking error of PMSM systems under flux linkage variations is shown in Fig. 7. $\psi_{r0}=0.41$ Wb is the nominal value of rotor flux. It can be observed that there is almost no effect on the tracking performance under different rotor fluxes. Thus, we can conclude that the proposed method has good robustness against external disturbances and internal uncertainties.
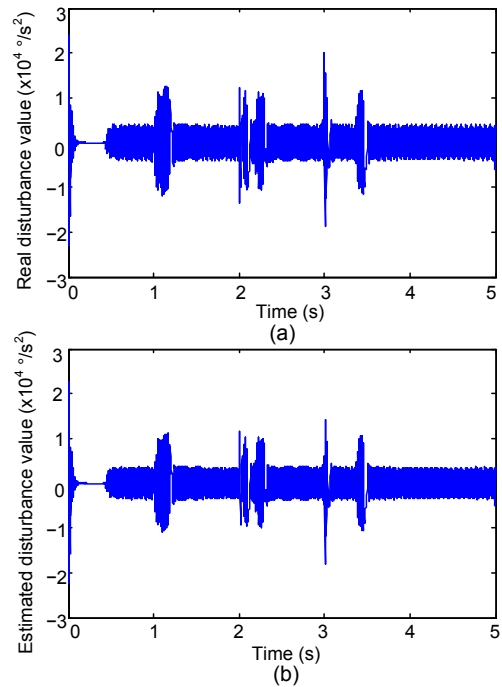
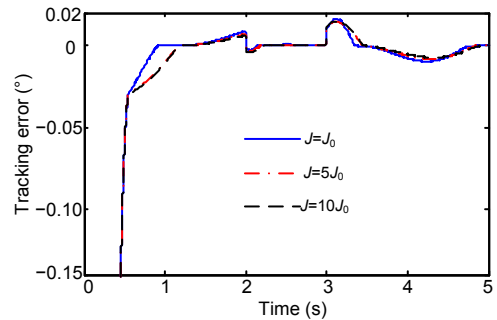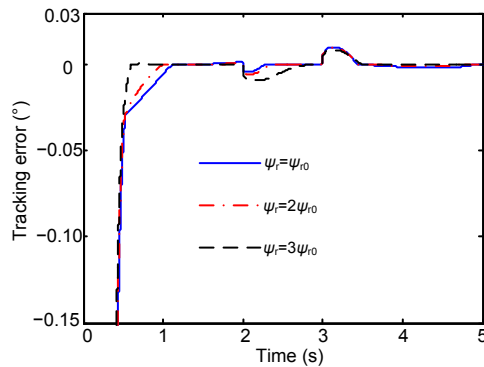**Fig. 5 Real (a) and estimated (b) disturbance values of the extended state observer**

**Fig. 6 Tracking performance of RFCISM under system inertia variations in simulation**

Fig. 7 Tracking performance of RFCISM under flux linkage variations in simulation

4.2 Experimental results

To further evaluate the effectiveness of the RFCISM method, an experimental setup for position control of PMSM is built (Fig. 8). The real-time emulator contains the DSP TMS320F28335PGFA (Texas Instruments). Its function is to provide a MATLAB/ Simulink programming environment. The whole algorithm, including position-speed control, Clarke transform, and inverse Park transform, is implemented by MATLAB/Simulink. Then, all the algorithms are converted into DSP codes. Next, the gate drive is sent from the DSP to the driver of PMSM. Experimental data can be collected on the host computer. All of the processes are supported by real-time simulation software named Links-RT (Beijing Linkstech Technology Co., Ltd.). The sampling times of the position-speed loop and current loop are 1.0 and 0.1 ms, respectively. An incremental position encoder is used to measure the rotor speed and absolute rotor position. Hall-effect devices are used to measure the phase currents.

Parameters of CNTSM are set as follows: $k_1=k_2=150$, $q_0=1$, $p_0=5$, $m=9$, $n=5$, and $\beta_2=1/120$.
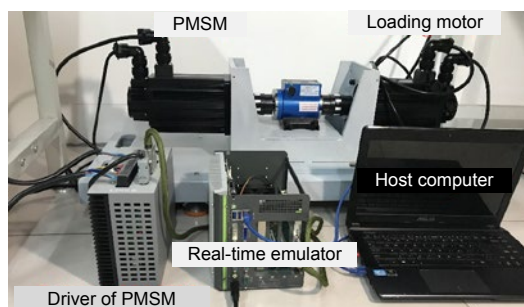
Fig. 8 Experimental test setup

PI parameters of the two current loops are the same, i.e., $K_p=5.7$ and $K_i=8.6$. Parameters of FCISM in the nonlinear phase are set as follows: $\beta_I=1/180$, $\alpha_I=200$, $\gamma_1=1.7$, $n_1=1$, $m_I=5$, $k_{1I}=k_{2I}=250$, $q_{0I}=1$, $p_{0I}=5$, and $\delta=1$. PI parameters of the two current loops are the same, i.e., $K_p=7.5$ and $K_i=12.5$. For RFCISM, the pole of the ESO is selected as $-p=-35\,000$ and other parameters are the same as those of FCISM.

First, we demonstrate the positioning performance of the proposed RFCISM. The position reference is set to $\theta_{ref}=70°$, which can lead to a good performance of the CNTSM controller. Performances of these three schemes are shown in Fig. 9 and summarized in Table 2. It is obvious that all these three control schemes can achieve finite-time stabilization, but the RFCISM can effectively depress the overshoot and shorten the settling time.
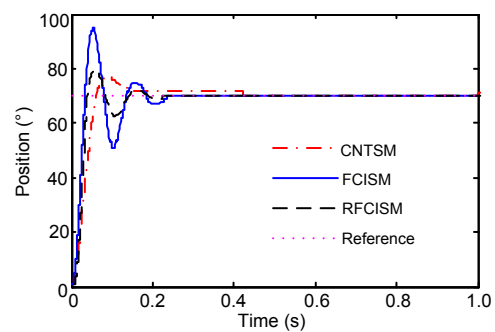
Fig. 9 Positioning performance of three methods for position reference $\theta_{ref}=70°$

Table 2 Positioning performance comparison of three control schemes

Control scheme	Overshoot (%)	Settling time (s)
CNTSM	10.0	0.42
FCISM	35.7	0.23
RFCISM	14.2	0.22

Then, the tracking performance of the proposed RFCISM is demonstrated. The position reference is $\theta_{ref}=30\cos[\pi/(2t)]°$, which is the same as that in the simulation. Load torque $T_L=15$ N·m is added at $t=2$ s and removed at $t=2.5$ s. Experimental results of CNTSM, FCISM, and RFCISM are shown in Figs. 10, 11, and 12, respectively. We can see that they match the simulation results well. The proposed RFCISM has fast response, precise tracking performance, and good robustness.
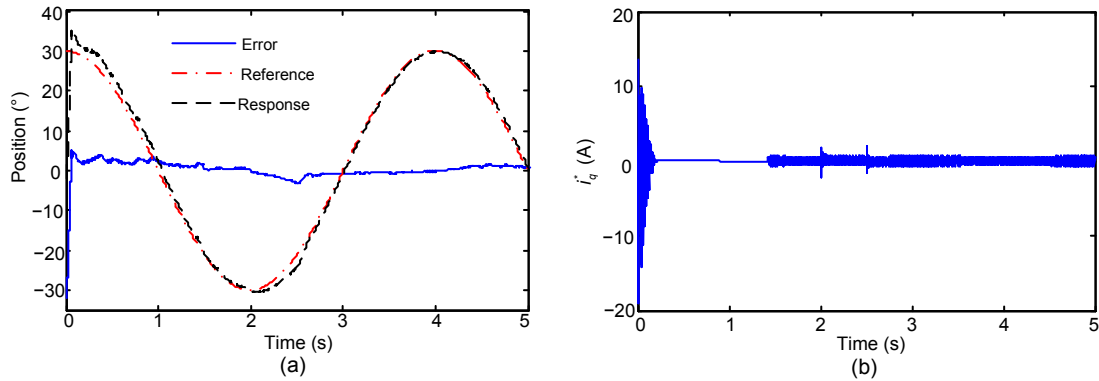
Fig. 10 Tracking performances of CNTSM in the experiment: (a) position response; (b) control input i_q^*
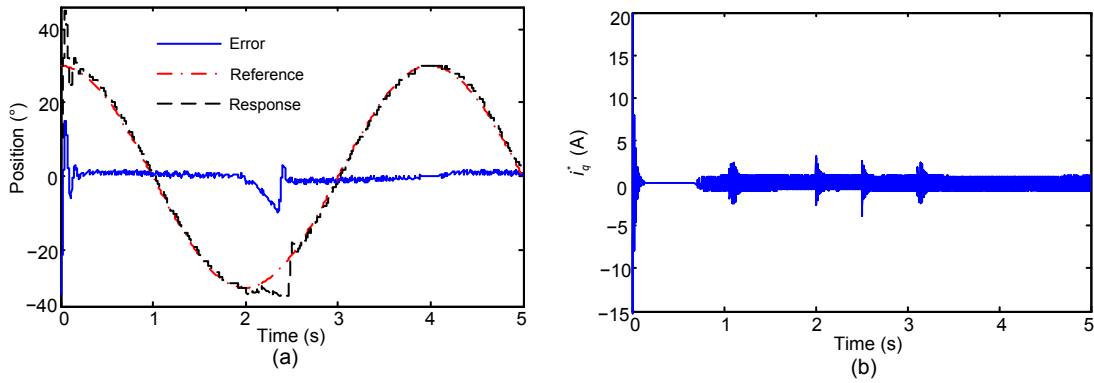

Fig. 11 Tracking performances of FCISM in the experiment: (a) position response; (b) control input i_q^*
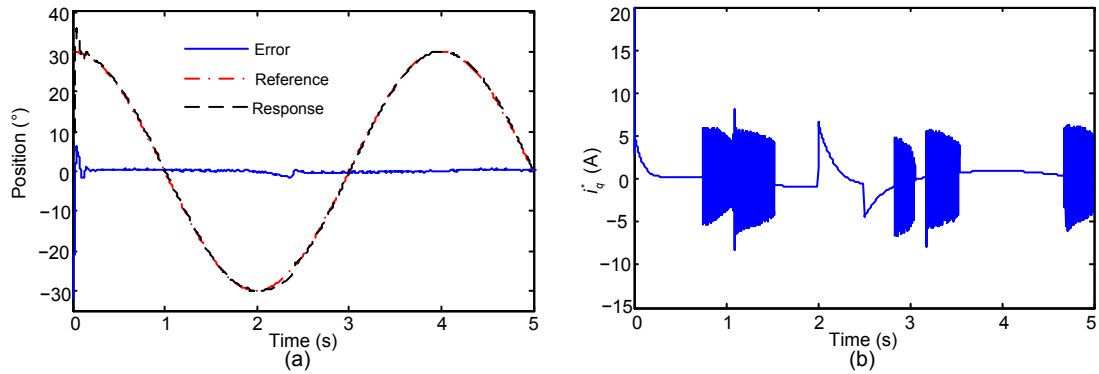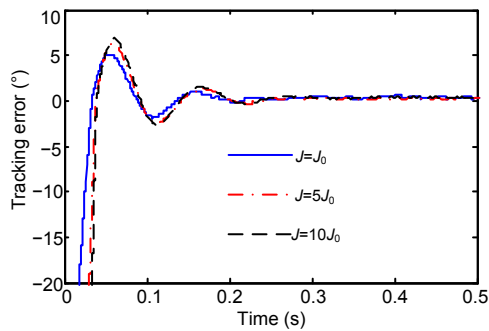

Fig. 12 Tracking performances of RFCISM in the experiment: (a) position response; (b) control input i_q^*

Fig. 13 shows the tracking error of the proposed method when the system inertia varies. We can see that the convergence speed becomes slower with the increase in the system inertia. However, the transient response remains fast and accurate regardless of the internal parameter variations. Thus, we can conclude that the proposed method has good robustness against internal uncertainties.

To validate the tracking range of the proposed method, three different position references are adopted, i.e., $\theta_{\text{ref}}=30\cos[\pi/(2t)]°$, $\theta_{\text{ref}}=60\cos[\pi/(2t)]°$, and $\theta_{\text{ref}}=90\cos[2\pi/(3t)]°$. Fig. 14 shows the experimental results. We can see that the overshoot and the settling time increase with the increase in amplification or frequency. However, the tracking performance remains desirable in all cases. It is evident that the proposed control system has superior performance in tracking a wide range of target positions.

Fig. 13 Tracking performance of RFCISM with perturbations in system inertia
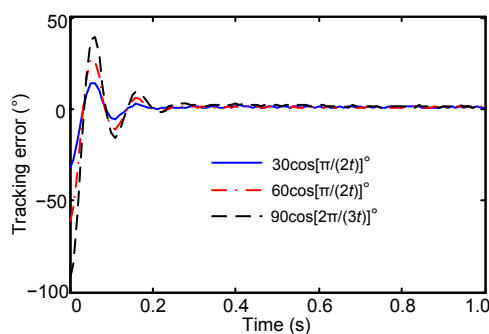
Fig. 14 Tracking performance of RFCISM for different position references

4.3 Discussion

To make comparisons, the simulation tracking performances of these three methods are summarized (Table 3). It can be observed that the settling time of RFCISM is reduced by 72.9% and that the steady tracking error is reduced by 90.9% compared with the CNTSM method. Experimental tracking performances are summarized in Table 4. We can see that the experimental results match simulation results well, and that the settling time, steady tracking error, and the maximum fluctuation of RFCISM are reduced by 85%, 58.7%, and 53.9%, respectively, compared with the CNTSM method. Thus, we can conclude that the RFCISM controller can realize faster response and better tracking than the conventional CNTSM method. In addition, the proposed method has superior robustness with respect to internal uncertainties and external disturbance.

Note that there is still some chattering in the control signals. However, it is well known that power converters have only the on–off operation mode. Therefore, chattering does not cause difficulty for practical electric drives. To eliminate the chattering

phenomenon in PMSM systems, the reaching law should be further improved in the future work.

Table 3 Simulation tracking performances of three control schemes

Control scheme	Settling time (s)	Steady tracking error (°)
CNTSM	1.70	0.11
FCISM	0.47	0.11
RFCISM	0.46	0.01

Table 4 Experimental tracking performances of three control schemes

Control scheme	Settling time (s)	Steady tracking error (°)	Maximum disturbance fluctuation (°)
CNTSM	1.20	1.50	3.21
FCISM	0.18	1.67	3.09
RFCISM	0.18	0.62	1.48

5 Conclusions

A fast-response and good-robustness sliding mode controller was proposed for position control of permanent magnet synchronous motor (PMSM) servo systems. Contributions of this study are listed as follows:

1. The conventional integral sliding surface was modified so that fast convergence can be obtained.

2. A continuous reaching law was applied in the controller design. Consequently, the chattering problem of the conventional sliding mode controller can be solved to some extent.

3. An extended state observer was adopted to estimate and compensate for system disturbances, so the disturbance rejection capability of PMSM systems can be improved remarkably.

Simulation and experimental results showed that the proposed RFCISM has fast response and accuracy in positioning and tracking. In addition, good robustness against inertial parameter variations and external load disturbances was obtained. This control scheme can be applied to other relevant servo systems.

experiments and processed the data. Jun-feng JIANG and Xiao-jun ZHOU revised and finalized the paper.

Compliance with ethics guidelines

Jun-feng JIANG, Xiao-jun ZHOU, Wei ZHAO, Wei LI, and Wen-dong ZHANG declare that they have no conflict of interest.

References

Al-Ghanimi A, Zheng J, Man Z, 2017. A fast non-singular terminal sliding mode control based on perturbation estimation for piezoelectric actuators systems. *Int J Contr*, 90(3):480-491.
https://doi.org/10.1080/00207179.2016.1185157

Baik IC, Kim KH, Youn MJ, 2000. Robust nonlinear speed control of PM synchronous motor using boundary layer integral sliding mode control technique. *IEEE Trans Contr Syst Technol*, 8(1):47-54.
https://doi.org/10.1109/87.817691

Barkat S, Tlemçani A, Nouri H, 2011. Noninteracting adaptive control of PMSM using interval type-2 fuzzy logic systems. *IEEE Trans Fuzzy Syst*, 19(5):925-936.
https://doi.org/10.1109/TFUZZ.2011.2152815

Bobtsov A, Bazylev D, Pyrkin A, et al., 2017. A robust nonlinear position observer for synchronous motors with relaxed excitation conditions. *Int J Contr*, 90(4):813-824.
https://doi.org/10.1080/00207179.2016.1230229

Chaoui H, Sicard P, 2012. Adaptive fuzzy logic control of permanent magnet synchronous machines with nonlinear friction. *IEEE Trans Ind Electron*, 59(2):1123-1133.
https://doi.org/10.1109/TIE.2011.2148678

Chen QH, Wang QF, Wang T, 2015. Optimization design of an interior permanent-magnet synchronous machine for a hybrid hydraulic excavator. *Front Inform Technol Electron Eng*, 16(11):957-968.
https://doi.org/10.1631/FITEE.1500056

Chiu CS, 2012. Derivative and integral terminal sliding mode control for a class of MIMO nonlinear systems. *Automatica*, 48(2):316-326.
https://doi.org/10.1016/j.automatica.2011.08.055

El-Sousy FFM, 2010. Hybrid H^∞-based wavelet-neural-network tracking control for permanent-magnet synchronous motor servo drives. *IEEE Trans Ind Electron*, 57(9):3157-3166.
https://doi.org/10.1109/TIE.2009.2038331

El-Sousy FFM, 2013. Intelligent optimal recurrent wavelet Elman neural network control system for permanent-magnet synchronous motor servo drive. *IEEE Trans Ind Inform*, 9(4):1986-2003.
https://doi.org/10.1109/TII.2012.2230638

Feng G, Liu YF, Huang LP, 2004. A new robust algorithm to improve the dynamic performance on the speed control of induction motor drive. *IEEE Trans Power Electron*, 19(6):1614-1627.
https://doi.org/10.1109/TPEL.2004.836619

Feng Y, Yu XH, Man ZH, 2002. Non-singular terminal sliding mode control of rigid manipulators. *Automatica*, 38(12):2159-2167.
https://doi.org/10.1016/S0005-1098(02)00147-4

Feng Y, Han FL, Yu XH, 2014. Chattering free full-order sliding-mode control. *Automatica*, 50(4):1310-1314.
https://doi.org/10.1016/j.automatica.2014.01.004

Han JQ, 2009. From PID to active disturbance rejection control. *IEEE Trans Ind Electron*, 56(3):900-906.
https://doi.org/10.1109/TIE.2008.2011621

Jiang JF, Zhou XJ, 2019. A robust and fast sliding mode controller for position tracking control of permanent magnetic synchronous motor. 3rd Int Conf on Power, Energy and Mechanical Engineering, p.95-99.
https://doi.org/10.1051/e3sconf/20199503002

Li SH, Liu ZG, 2009. Adaptive speed control for permanent-magnet synchronous motor system with variations of load inertia. *IEEE Trans Ind Electron*, 56(8):3050-3059.
https://doi.org/10.1109/TIE.2009.2024655

Li SH, Sun HB, Yang J, et al., 2015. Continuous finite-time output regulation for disturbed systems under mismatching condition. *IEEE Trans Autom Contr*, 60(1):277-282. https://doi.org/10.1109/TAC.2014.2324212

Man ZH, Paplinski AP, Wu HR, 1994. A robust MIMO terminal sliding mode control scheme for rigid robotic manipulators. *IEEE Trans Autom Contr*, 39(12):2464-2469.
https://doi.org/10.1109/9.362847

Miklosovic R, Gao ZQ, 2004. A robust two-degree-of-freedom control design technique and its practical application. IEEE Industry Applications Conf, p.1495-1502.
https://doi.org/10.1109/IAS.2004.1348669

Nguyen AT, Rafaq MS, Choi HH, et al., 2018. A model reference adaptive control based speed controller for a surface-mounted permanent magnet synchronous motor drive. *IEEE Trans Ind Electron*, 65(12):9399-9409.
https://doi.org/10.1109/TIE.2018.2826480

Nguyen HT, Jung JW, 2018. Finite control set model predictive control to guarantee stability and robustness for surface-mounted PM synchronous motors. *IEEE Trans Ind Electron*, 65(11):8510-8519.
https://doi.org/10.1109/TIE.2018.2814006

Saadaoui O, Khlaief A, Abassi M, et al., 2017. A sliding-mode observer for high-performance sensorless control of PMSM with initial rotor position detection. *Int J Contr*, 90(2):393-408.
https://doi.org/10.1080/00207179.2016.1181788

Su JB, Qiu WB, Ma HY, et al., 2004. Calibration-free robotic eye-hand coordination based on an auto disturbance-rejection controller. *IEEE Trans Robot*, 20(5):899-907.
https://doi.org/10.1109/TRO.2004.829458

Su YX, Zheng CH, Duan BY, 2005. Automatic disturbances rejection controller for precise motion control of permanent-magnet synchronous motors. *IEEE Trans Ind Electron*, 52(3):814-823.
https://doi.org/10.1109/TIE.2005.847583

Wai RJ, 2001. Total sliding-mode controller for PM synchronous servo motor drive using recurrent fuzzy neural

network. *IEEE Trans Ind Electron*, 48(5):926-944.
https://doi.org/10.1109/41.954557

Wang HM, Li SH, Lan QX, et al., 2017. Continuous terminal sliding mode control with extended state observer for PMSM speed regulation system. *Trans Inst Meas Contr*, 39(8):1195-1204.
https://doi.org/10.1177/0142331216630361

Wang M, Yang JQ, Zhang X, et al., 2018. Accurate two-degree-of-freedom discrete-time current controller design for PMSM using complex vectors. *Front Inform Technol Electron Eng*, 19(4):569-581.
https://doi.org/10.1631/FITEE.1601390

Wu D, Chen K, Wang XK, 2007. Tracking control and active disturbance rejection with application to noncircular machining. *Int J Mach Tool Manuf*, 47(15):2207-2217.
https://doi.org/10.1016/j.ijmachtools.2007.07.002

Yang J, Li SH, Su JY, et al., 2013. Continuous nonsingular terminal sliding mode control for systems with mismatched disturbances. *Automatica*, 49(7):2287-2291.
https://doi.org/10.1016/j.automatica.2013.03.026

Yang JQ, Yin RS, Zhang XJ, et al., 2017. Exponential response electrical pole-changing method for a five-phase induction machine with a current sliding mode control strategy. *Front Inform Technol Electron Eng*, 18(8):1151-1166.
https://doi.org/10.1631/FITEE.1601728

Yu SH, Yu XH, Shirinzadeh B, et al., 2005. Continuous finite-time control for robotic manipulators with terminal sliding mode. *Automatica*, 41(11):1957-1964.
https://doi.org/10.1016/j.automatica.2005.07.001

Zeng ZL, Cheng LM, Qian L, et al., 2002. A newly robust controller design for the position control of permanent-magnet synchronous motor. *IEEE Trans Ind Electron*, 49(3):558-565.
https://doi.org/10.1109/TIE.2002.1005380

Zhang XY, 2016. Application of direct adaptive fuzzy sliding mode control into a class of non-affine discrete nonlinear systems. *Front Inform Technol Electron Eng*, 17(12): 1331-1343. https://doi.org/10.1631/FITEE.1500318

Zhi DW, Xu L, Williams BW, 2010. Model-based predictive direct power control of doubly fed induction generators. *IEEE Trans Power Electron*, 25(2):341-351.
https://doi.org/10.1109/TPEL.2009.2028139